

Higher-order topological insulator phase in a modified Haldane modelBaokai Wang^{1,*}, Xiaoting Zhou^{1,*}, Hsin Lin,² and Arun Bansil^{1,†}¹*Department of Physics, Northeastern University, Boston, Massachusetts 02115, USA*²*Institute of Physics, Academia Sinica, Taipei 11529, Taiwan* (Received 20 April 2021; revised 3 August 2021; accepted 30 August 2021; published 17 September 2021)

We explore the topological properties of a modified Haldane model (MHM) in which the strength of the nearest-neighbor and next-nearest-neighbor hopping terms is made unequal and the threefold rotational symmetry C_3 is broken by introducing a dimerization term ($|t_{1w(2w)}| < t_{1s(2s)}$) in the Hamiltonian. Using the parameter $\eta = t_{1w}/t_{1s} = t_{2w}/t_{2s}$, we show that this MHM supports a transition from the quantum anomalous Hall insulator to a higher-order topological insulator (HOTI) phase at $\eta = \pm 0.5$. It also hosts a zero-energy corner mode on a nanodisk that can transition to a trivial insulator without gap closing when the inversion symmetry is broken. The gap-closing critical states are found to be magnetic semimetals with a single Dirac node which, unlike the classic Haldane model, can move along the high-symmetry lines in the Brillouin zone. Our MHM offers a rich tapestry of HOTIs and other topological and nontopological phases.

DOI: [10.1103/PhysRevB.104.L121108](https://doi.org/10.1103/PhysRevB.104.L121108)

Introduction. The discovery of topological insulators (TIs) [1–4] has triggered a rapidly developing research field. The signature of a d -dimensional TI is the emergence of robust, symmetry-protected gapless states on its $(d - 1)$ -dimensional boundaries. Recently, topological insulators with higher-order bulk-boundary correspondences have also been discovered, which are dubbed as higher-order topological insulators (HOTIs) [5,6]. A HOTI exhibits a gapped $(d - 1)$ -dimensional boundary and supports topologically protected states on a lower, $(d - n)$ -dimensional boundary where $n \geq 2$. For example, a three-dimensional (3D) HOTI exhibits two-dimensional (2D) gapped surfaces and topologically protected states on its one-dimensional (1D) hinges. Similarly, a 2D HOTI hosts nontrivial states on the zero-dimensional (0D) corners of a nanodisk rather than the gapless propagating 1D edge states. HOTIs have been proposed and realized in a variety of 3D and 2D materials [5–41], as well as in photonic and phononic systems [42–60], quasicrystals [61], amorphous systems [62,63], heterostructures [64,65], magnetic compounds [66–68], topoelectrical circuits [69–71], interacting fermion and boson systems [72–78], and non-Hermitian [79–86] and other systems [87–100].

The Haldane model, which has become a classic in the field of topological materials, realizes the quantum Hall effect on a honeycomb lattice without an external magnetic field [101], and thus hosts a quantum anomalous Hall insulator (QAHI) state. The introduction of magnetic phases ϕ on the next-nearest-neighbor (NNN) hoppings breaks the time-reversal symmetry \mathcal{T} of the Haldane model without generating a net magnetic flux in the plaquettes. Here, we discuss a modified Haldane model (MHM) in which the threefold rotational symmetry C_3 is broken via dimerization along the \hat{y} direction

as shown in Fig. 1(a), where t_{1s} and t_{2s} are the hopping parameters for the $\pm\delta_1$ bonds and $\pm\mathbf{a}_{1,2}$ are the lattice vectors, respectively. The other hopping parameters are labeled as $t_{(1,2)w}$. We define the parameter $\eta = t_{1w(2w)}/t_{1s(2s)}$, and obtain the full phase diagram for our MHM in the three-dimensional (m, ϕ, η) parameter space, where m is the inversion-breaking on-site potential term. We find that due to the breaking of \mathcal{T} ($\phi \neq 0, \pm\pi$), the critical gap-closing states are semimetals with a single Dirac node. When m is zero, phase transitions accompanying band-gap closing and reopening are observed at $\eta = \pm 0.5$ from a QAHI to an insulating phase with zero Chern number which we show to be a HOTI [Fig. 1(b)] protected by inversion symmetry.

For any 2D insulator with a zero Chern number ($C = 0$), Wannier functions (WFs) of the occupied bands [102] can be used to identify topologically nontrivial states. The symmetric WFs associated with smooth and symmetric Bloch wave functions may or may not be well defined [103] and, in general, a set of symmetric WFs cannot be found for all the occupied bands in a nontrivial insulator [104,105]. Note that there is a *mismatch* between the Wannier centers (WCs) and the lattice sites [7,8,106] in nontrivial states. WCs can be formulated in terms of d -dimensional polarization [107–109]. The position of a WC is tied to a symmetric invariant point and the projection is quantized, so that it can serve as a topological index for defining a topological insulator.

We will explore the evolution of topological states on various edges on our MHM by examining the locations of WCs and their mismatch with the lattice sites and the associated polarizations $p_{\alpha=x,y}$ [11]. A quantized nonzero polarization indicates that the insulator is nontrivial. Finally, the HOTI phase is identified through the emergence of in-gap zero-energy modes in a properly designed nanodisk: When one electron is added in the zero mode, a fractional charge appears at each corner as expected for a 2D HOTI [Fig. 1(b)]. Interestingly, the trivial insulator is found to transition to the

*These authors contributed equally to this work.

†ar.bansil@northeastern.edu

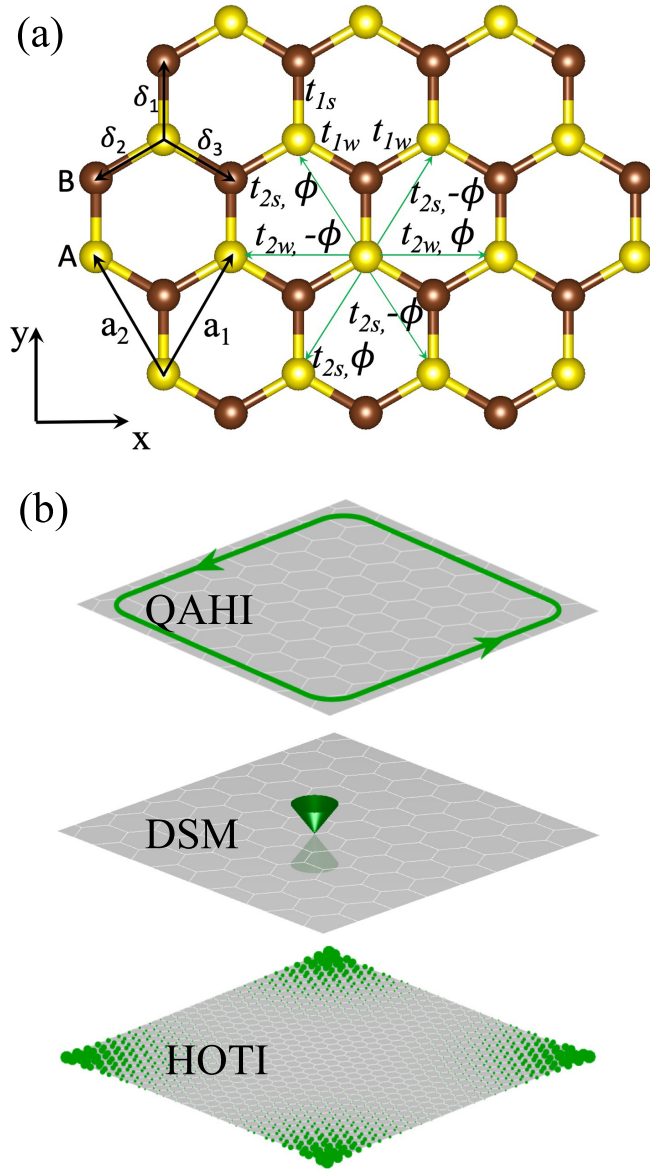


FIG. 1. (a) Our modified Haldane model with A (yellow) and B (brown) sublattices. \mathbf{a}_1 and \mathbf{a}_2 denote lattice translation vectors and $t_{1s,1w}$ ($t_{2s,2w}$) are the NN (NNN) hopping parameters, where t_{1s} (t_{2s}) is assumed to be greater than t_{1w} (t_{2w}). ϕ is the magnetic phase. (b) Phase transitions realized in the model range from a QAHI to a HOTI via a critical semimetal phase that hosts a single Dirac cone.

HOTI without a gap closing along certain paths in the phase space.

Modified Haldane model and the associated phase diagram. We start by commenting on the Haldane model, which was proposed for the realization of a QAHI or a Chern insulator on a honeycomb lattice in the absence of an external magnetic field [101]. The key insight is the introduction of a time-reversal breaking phase ϕ on the NNN hopping terms [Fig. 1(a)], which induce zero net magnetic flux in the plaquettes, so that the translational symmetry of the system is preserved. The threefold rotational symmetry C_3 is also preserved in the model because the NN and NNN hopping strengths are equal, i.e., $t_1 = t_{1s} = t_{1w}$ and $t_2 = t_{2s} = t_{2w}$

[Fig. 1(a)]. The Haldane model Hamiltonian can be written as

$$H = t_1 \sum_{\langle i,j \rangle} c_i^\dagger c_j + t_2 \sum_{\langle\langle i,j \rangle\rangle} e^{-iv_{ij}\phi} c_i^\dagger c_j + m \sum_i \epsilon_i c_i^\dagger c_i. \quad (1)$$

Here, $v_{i,j} = \text{sign}(\hat{d}_1 \times \hat{d}_2)_z = \pm 1$ accounts for the alternating sign of the magnetic phase, with $\hat{d}_{1,2}$ being the vectors along the two NNN bonds. m is the inversion-breaking on-site potential. $\epsilon_i = +1$ (-1) when i refers to the A (B) sublattice sites. In the Haldane model, the phase transition between a QAHI and a trivial insulator occurs when $m = \pm 3\sqrt{3}t_2 \sin \phi$, and the gap closing and reopening takes place at the C_3 symmetric points K and K' .

We turn now to consider the MHM, which involves making the NN and NNN hopping strengths unequal as shown in Fig. 1(a), where $|t_{1w(2w)}| < t_{1s(2s)}$. This is equivalent to applying a uniaxial strain to the honeycomb lattice along the x direction [110]. As a result, C_3 is broken and the Hamiltonian takes the form $H(\mathbf{k}) = \sum_{i=0}^3 d_i(\mathbf{k})\sigma_i$. Here, σ_0 and σ are the identity matrix and the three Pauli matrices acting in the sublattice space. The $d_i(\mathbf{k})$ terms can be expressed as

$$\begin{aligned} d_0 &= 2 \cos \phi [t_{2s}(\cos \mathbf{k} \cdot \mathbf{a}_1 + \cos \mathbf{k} \cdot \mathbf{a}_2) \\ &\quad + t_{2w} \cos \mathbf{k} \cdot (\mathbf{a}_1 - \mathbf{a}_2)], \\ d_1 &= t_{1s} \cos \mathbf{k} \cdot \delta_1 + t_{1w}(\cos \mathbf{k} \cdot \delta_2 + \cos \mathbf{k} \cdot \delta_3), \\ d_2 &= t_{1s} \sin \mathbf{k} \cdot \delta_1 + t_{1w}(\sin \mathbf{k} \cdot \delta_2 + \sin \mathbf{k} \cdot \delta_3), \\ d_3 &= 2 \sin \phi [t_{2s}(\sin \mathbf{k} \cdot \mathbf{a}_1 - \sin \mathbf{k} \cdot \mathbf{a}_2) \\ &\quad - t_{2w} \sin \mathbf{k} \cdot (\mathbf{a}_1 - \mathbf{a}_2)] + m. \end{aligned} \quad (2)$$

We can understand the topological features of the MHM by examining the gap-closing/reopening transitions. For this purpose, we introduce the new parameter $\eta = t_{1w}/t_{1s} = t_{2w}/t_{2s}$ and work out a generalized phase diagram in the 3D parameter space of (m, ϕ, η) as shown in Fig. 2(a), where $\phi \in [-\pi, \pi]$, and $\eta \in [-1, 1]$. Our analysis shows that the gap-closing phase transition occurs at

$$m = \pm 3t_{2s} \sin \phi \sqrt{4 - \frac{1}{\eta^2}}. \quad (3)$$

In Fig. 2(a), at each η value in the regions $\eta \in [-1, -1/2) \cup (1/2, 1]$, Eq. (3) describes two sinusoids (denoted by signs $+$ and $-$) with η -dependent amplitudes, which separate the QAHI phase enclosed by the curves and the insulating phase with zero Chern number. The $+$ and $-$ sinusoids are seen to merge into a line at $\eta = \pm 1/2$, leading to two sets of pocketlike sinusoidal surfaces.

The phases on the sinusoidal surfaces represent Dirac semimetals (DSMs) that host a single Dirac node (DN) if \mathcal{T} is broken. Otherwise, the \mathcal{T} symmetry enforces the appearance of a pair of Dirac nodes. The location of the Dirac nodes depends only on η in all cases. In the standard Haldane model ($\eta = 1$), the DN is locked at the corner of the Brillouin zone (BZ) by the C_3 symmetry. However, in the MHM, C_3 is broken, and the DN is no longer pinned at the C_3 symmetric points K and K' . In contrast, as η varies from 1 to $1/2$, the DN for the $+$ ($-$) sinusoid moves from $K \rightarrow M$ ($K' \rightarrow M$). The two DNs meet at the M point and gap up at $\eta = 1/2$, leading to the transition to the insulating phases. At $\eta = -1/2$, the

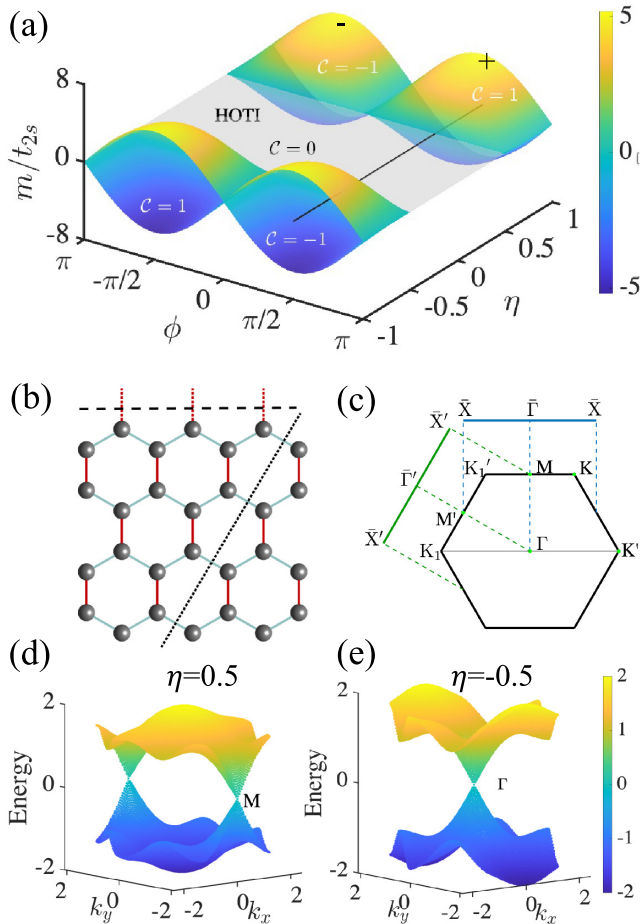


FIG. 2. (a) Phase diagram of the MHM. The black line denotes the path along which a phase transition QAH($C=1$)-HOTI-QAH($C=-1$) can occur. + and - signs label the two sinusoids discussed in the text. (b) Honeycomb lattice with two types of zigzag edges labeled by the dashed and dotted lines, which cut strong (red) and weak (cyan) bonds, respectively. (c) The Brillouin zone and its projections on the two types of zigzag directions marked in (b). (d), (e) Band structures of the critical semimetal phases which host a single Dirac node at (d) the M point when $\eta = 0.5$, and (e) the Γ point when $\eta = -0.5$. Parameters used in the results of (d) and (e) are $t_{1s} = 1.0$, $t_{2s} = 0.3$, $m = 0$, and $\phi = \pi/2$.

DSM phases reappear with the DN lying at the Γ point. As η decreases, the DN for the + (-) sinusoid moves from $\Gamma \rightarrow K'$ ($\Gamma \rightarrow K_1$). When the two sinusoids meet at $\phi = 0$ or $\pm\pi$, \mathcal{T} is restored and connects the two DNs.

We emphasize that the existence of the DN does not require symmetries, although its location is restricted by the preserved symmetries [111]. In MHM, the symmetry $\mathcal{M}_x * \mathcal{T}$ (a combination of time-reversal and mirror symmetry normal to the x axis) is the only symmetry preserved in all states. Therefore, the single DNs are restricted to lie on the symmetry-invariant lines, $K'_1 - M - K$ and $K_1 - \Gamma - K'$.

One might guess that any two phases in regions away from the pockets in Fig. 2(a) would continuously deform into each other without a gap closing and would thus share the same topology. However, this turns out not to be the case because the symmetries involved differ in the parameter space away

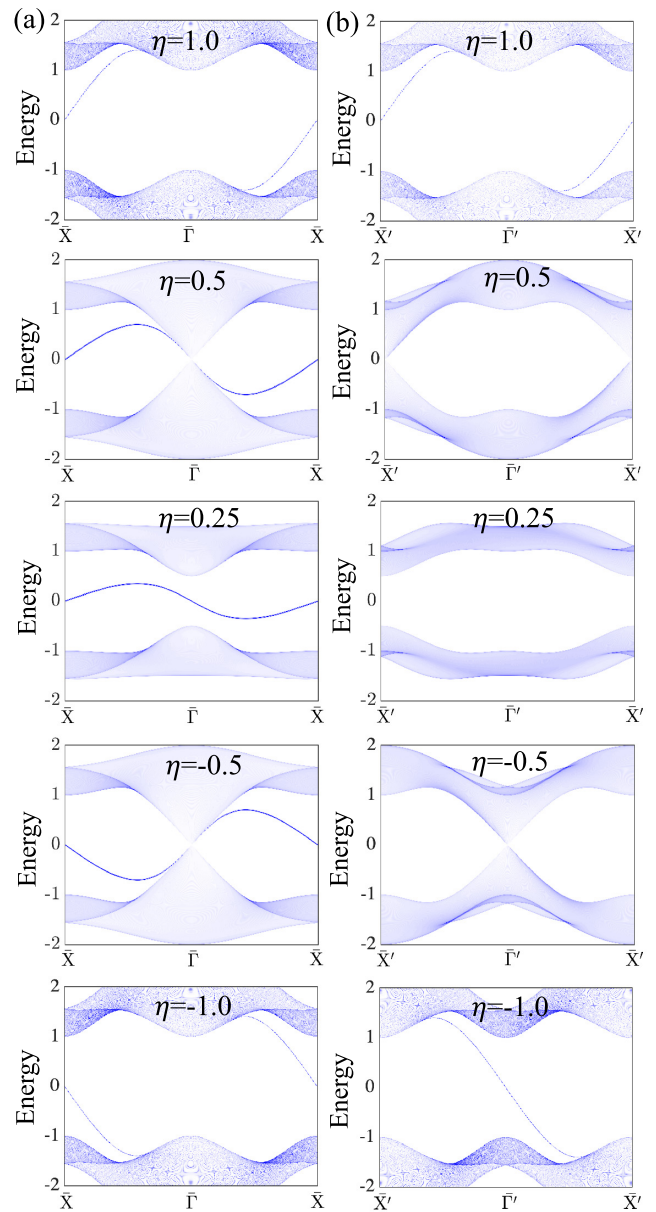


FIG. 3. Evolution of the band structures for the two types of zigzag nanoribbon edges [dotted and dashed lines in Fig. 2(b)]: (a) strong-bond-cutting edge and (b) weak-bond-cutting edge. The computations are based on a semi-infinite nanoribbon using a Green's function method. Parameters used in the computations are $t_{1s} = 1.0$, $t_{2s} = 0.3$, $m = 0$, and $\phi = \pi/2$.

from the pockets, so that a phase transition can occur without a gap closing. Therefore, it is interesting to identify the preserved symmetries in the various regions of the parameter space.

We first focus on the inversion-symmetric plane with $m = 0$. We start from the QAH ($\eta = 1$) at $\phi = \pi/2$, and trace the transitions along the path given by the black line in Fig. 2(a). As η varies, the gap closes and reopens at $\eta = \pm 1/2$, indicating transitions from a QAH to an unknown insulating phase when $\eta \in (-1/2, 1/2)$ with Chern number $C = 0$. Insight into the nature of the states involved here is provided by Figs. 3(a) and 3(b), which show how the band structure evolves with

varying η in nanoribbons with zigzag edges cutting the strong and weak bonds, respectively. Over the range $\eta \in (0.5, 1]$, both nanoribbons are seen to support only one chiral gapless edge mode around \bar{X} or \bar{X}' and the MHM remains a QAHI ($C = 1$). At $\eta = 0.5$, the band gap vanishes, leading to the emergence of a single Dirac node [Fig. 2(d)], which is pinned at the M point due to \mathcal{I} symmetry. (This Dirac node is located at the K or K' point in the regular Haldane model.) This indicates the presence of a distinct band inversion, and implies that MHM may go into a nontrivial insulating phase, which is also suggested by the evolution of the edge states in Figs. 3(a) and 3(b). Since the M point of the bulk BZ is projected to the $\bar{\Gamma}$ (\bar{X}') point as seen from the dashed (dotted) line in Fig. 2(b), the corresponding edge states are essentially different. For the weak-bond cut (dotted line), when the band gap closes at \bar{X}' , the gapless edge mode is absorbed by bulk bands, and does not reappear when the gap reopens. But, for the strong-bond-cutting edge (dashed line), the edge mode survives. Unlike the topological edge mode of the QAHI, the edge mode here is detached from the bulk states and it is not topological. As η changes sign and another band closing and reopening takes place at the $\bar{\Gamma}$ point for $\eta = -0.5$, the MHM transitions back into a Chern insulator, accompanied with a chiral gapless edge mode propagating in the opposite direction ($C = -1$).

Comparing the two types of edge states, the strong-bond cut supports an in-gap edge mode, but not the weak-bond cut, which suggests that in this insulating phase the WCs may be located at the strong and not the weak bonds. In other words, the in-gap edge mode can be expected only for the edges that cut through the strong bonds (see Supplemental Material for more discussions [111]).

Wannier centers and higher-order topology. In order to identify the topology of the insulator for $\eta \in (-0.5, 0.5)$, we discuss first the WCs associated with the various phases on the $m = 0$ plane. The WC, given by the polarization (p_x, p_y) , describes the average position of the charge in a unit cell. The polarization can be written as

$$p_{\alpha=x,y} = -\frac{1}{V} \int_{\text{BZ}} d\mathbf{k} A_{\alpha}, \quad (4)$$

where $A_{\alpha} = -i\langle \psi | \partial_{k_{\alpha}} | \psi \rangle$ is the Berry connection, V is the volume of the BZ, and the integration is over the whole BZ [7–9, 11]. Due to gauge invariance, the polarization is defined as $p_{\alpha} \bmod \mathbf{a}_i$, where \mathbf{a}_i are lattice translation vectors. As expected, our calculations reveal that the WC lies at the center of the strong bond. In general, since the WFs are symmetric, WCs should be located at the invariant points of the symmetry employed. On the $m = 0$ plane, the inversion symmetry \mathcal{I} remains intact and ties the WC to the center of the strong bond, which is inversion invariant. The mismatch between the quantized WCs and the atomic sites serves as a topological index to characterize the associated higher-order topology. Notably, this kind of a phase has been referred to as an obstructed atomic insulator in the literature [105].

Away from the inversion-symmetric plane ($m \neq 0$), the WC will move toward the lattice site A (B) if $m > 0$ ($m < 0$). When $|m|$ goes to infinity, the WC moves to the lattice site and the system transitions into an atomic insulator. Note that, in this case, the only symmetry preserved is $\mathcal{M}_x * \mathcal{T}$, under which p_y cannot be quantized. In other words, as \mathcal{I} symmetry

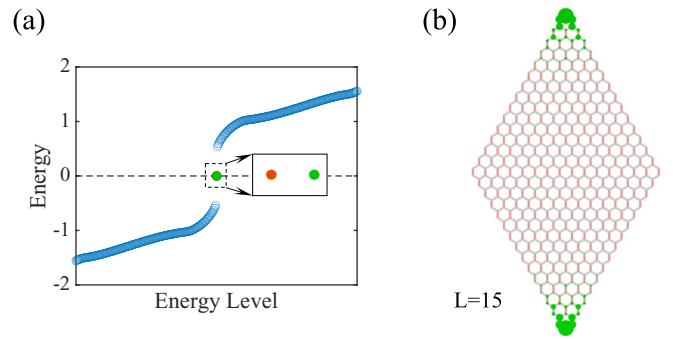


FIG. 4. (a) Energy spectrum of the nanodisk we considered when the system is in the HOTI phase. Two in-gap zero-energy modes (red and green dots) are shown. (b) Charge distribution of the zero-energy mode indicates that if one mode (marked in green) is filled with one electron, a fractional $1/2$ electron will be distributed at each of the two corners.

is broken, a phase transition occurs from a HOTI to a trivial insulator without gap closing.

A HOTI exhibits 0D zero-energy corner modes in a properly designed nanodisk (Fig. 4). In our case, the zero-energy corner states are protected by the particle-hole symmetry (PHS) defined by the antiunitary operator $\mathcal{C} = \sigma_3 \mathcal{K}$, where \mathcal{K} is the complex conjugate operator [112]. Since we are required to have $\mathcal{C}H(k)\mathcal{C}^{-1} = -H(-k)$, the PHS is preserved in our MHM only if both d_0 ($\phi = \pm\pi/2$) and m are zero. Otherwise, in the absence of PHS ($d_0 \neq 0$) with the inversion symmetry preserved ($m = 0$), the modes can be pushed away from zero energy but will remain degenerate. In this sense, the system is still nontrivial because the WC (Berry connection) is insensitive to the d_0 term. However, in the absence of inversion symmetry ($m \neq 0$), the WC is not well defined, and the degeneracy of the corner modes is lifted and the system becomes a trivial insulator, as discussed above.

We have computed the eigenstates of a rhombus-shaped nanodisk [Fig. 4(b)] of size $L = 15$, where L is the number of benzene rings on each side. Figure 4(a) shows the energy levels. There are two degenerate in-gap zero-energy modes (green and orange dots). If either of these two modes is filled with an electron, $1/2$ electron charge is distributed at each of the two corners [see Fig. 4(b)].

Conclusion. We explore the topological properties of a modified Haldane model (MHM) in which we have made the hopping strength unequal between the NN and NNN terms and broken the threefold rotational symmetry \mathcal{C}_3 of the Hamiltonian. This MHM is found to harbor a different nontrivial insulating phase on the inversion-symmetric plane, which can transition to the trivial insulator state without gap closing. The HOTI nature of the nontrivial phase is demonstrated by showing that the quantized Wannier centers, which are enforced by the inversion symmetry, do not lie at the lattice sites. The 2D HOTI state features a zero-dimensional, zero-energy corner mode, which is confirmed by computing the spectrum of a properly designed nanodisk. Interestingly, we find that the HOTI phase can transition to a trivial insulator without gap closing along certain paths in the phase space. The gap-closing critical states are magnetic semimetals with

a single Dirac node, which is not constrained to lie at the high-symmetry points in the BZ as is the case in the standard Haldane model. Regarding the experimental realization of our MHM, we note that pristine and generalized Haldane models have already been realized in optical lattices [113–116]: The parameter space of our MHM could be accessed by adjusting phase differences, frequencies, and/or intensities of the lasers involved [117]. Therefore, we expect our MHM to be amenable to implementation in an appropriately engineered optical lattice. Our MHM provides a rich playground for exploring HOTI and other topological and nontopological

phases and how transitions can be induced between these phases by varying the parameters in the model.

H.L. acknowledges the support by the Ministry of Science and Technology (MOST) in Taiwan under Grant No. MOST109-2112-M-001-014-MY3. The work at Northeastern University is supported by the Air Force Office of Scientific Research under Award No. FA9550-20-1-0322, and it benefited from computational resources of Northeastern University's Advanced Scientific Computation Center (ASCC) and the Discovery Cluster.

-
- [1] A. Bansil, H. Lin, and T. Das, *Rev. Mod. Phys.* **88**, 021004 (2016).
- [2] M. Z. Hasan and C. L. Kane, *Rev. Mod. Phys.* **82**, 3045 (2010).
- [3] X.-L. Qi and S.-C. Zhang, *Rev. Mod. Phys.* **83**, 1057 (2011).
- [4] N. P. Armitage, E. J. Mele, and A. Vishwanath, *Rev. Mod. Phys.* **90**, 015001 (2018).
- [5] F. Schindler, Z. Wang, M. G. Vergniory, A. M. Cook, A. Murani, S. Sengupta, A. Y. Kasumov, R. Deblock, S. Jeon, I. Drozdov, H. Bouchiat, S. Guéron, A. Yazdani, B. A. Bernevig, and T. Neupert, *Nat. Phys.* **14**, 918 (2018).
- [6] W. A. Benalcazar, B. A. Bernevig, and T. L. Hughes, *Phys. Rev. B* **96**, 245115 (2017).
- [7] M. Ezawa, *Phys. Rev. B* **98**, 045125 (2018).
- [8] M. Ezawa, *Phys. Rev. Lett.* **120**, 026801 (2018).
- [9] S. Franca, J. van den Brink, and I. C. Fulga, *Phys. Rev. B* **98**, 201114(R) (2018).
- [10] M. Geier, L. Trifunovic, M. Hoskam, and P. W. Brouwer, *Phys. Rev. B* **97**, 205135 (2018).
- [11] W. A. Benalcazar, B. A. Bernevig, and T. L. Hughes, *Science* **357**, 61 (2017).
- [12] M. Ezawa, *Phys. Rev. B* **97**, 241402(R) (2018).
- [13] E. Khalaf, *Phys. Rev. B* **97**, 205136 (2018).
- [14] F. K. Kunst, G. van Miert, and E. J. Bergholtz, *Phys. Rev. B* **97**, 241405(R) (2018).
- [15] G. van Miert and C. Ortix, *Phys. Rev. B* **98**, 081110(R) (2018).
- [16] W. A. Benalcazar, T. Li, and T. L. Hughes, *Phys. Rev. B* **99**, 245151 (2019).
- [17] R. Okugawa, S. Hayashi, and T. Nakanishi, *Phys. Rev. B* **100**, 235302 (2019).
- [18] M. Ezawa, *Nat. Mater.* **18**, 1266 (2019).
- [19] S. N. Kempkes, M. R. Slot, J. J. van den Broeke, P. Capiod, W. A. Benalcazar, D. Vanmaekelbergh, D. Bercioux, I. Swart, and C. Morais Smith, *Nat. Mater.* **18**, 1292 (2019).
- [20] B. Liu, G. Zhao, Z. Liu, and Z. F. Wang, *Nano Lett.* **19**, 6492 (2019).
- [21] T. Mizoguchi, H. Araki, and Y. Hatsugai, *J. Phys. Soc. Jpn.* **88**, 104703 (2019).
- [22] M. Ezawa, *Phys. Rev. Lett.* **121**, 116801 (2018).
- [23] C.-H. Hsu, P. Stano, J. Klinovaja, and D. Loss, *Phys. Rev. Lett.* **121**, 196801 (2018).
- [24] X. Zhang, Z.-K. Lin, H.-X. Wang, Z. Xiong, Y. Tian, M.-H. Lu, Y.-F. Chen, and J.-H. Jiang, *Nat. Commun.* **11**, 65 (2020).
- [25] L. B. Drissi and E. H. Saidi, *J. Phys.: Condens. Matter* **32**, 365704 (2020).
- [26] L. Trifunovic and P. W. Brouwer, *Phys. Rev. X* **9**, 011012 (2019).
- [27] F. Schindler, M. Brzezińska, W. A. Benalcazar, M. Iraola, A. Bouhon, S. S. Tsirkin, M. G. Vergniory, and T. Neupert, *Phys. Rev. Research* **1**, 033074 (2019).
- [28] X.-L. Sheng, C. Chen, H. Liu, Z. Chen, Z.-M. Yu, Y. X. Zhao, and S. A. Yang, *Phys. Rev. Lett.* **123**, 256402 (2019).
- [29] H. Fan, B. Xia, L. Tong, S. Zheng, and D. Yu, *Phys. Rev. Lett.* **122**, 204301 (2019).
- [30] D. Călugăru, V. Juričić, and B. Roy, *Phys. Rev. B* **99**, 041301(R) (2019).
- [31] Q.-B. Zeng, Y.-B. Yang, and Y. Xu, *Phys. Rev. B* **101**, 241104(R) (2020).
- [32] Y. Tanaka, R. Takahashi, and S. Murakami, *Phys. Rev. B* **101**, 115120 (2020).
- [33] S. K. Radha and W. R. L. Lambrecht, *Phys. Rev. B* **102**, 115104 (2020).
- [34] Y. Liu, Y. Wang, N. C. Hu, J. Y. Lin, C. H. Lee, and X. Zhang, *Phys. Rev. B* **102**, 035142 (2020).
- [35] Y. Ren, Z. Qiao, and Q. Niu, *Phys. Rev. Lett.* **124**, 166804 (2020).
- [36] M. Ezawa, *Phys. Rev. Research* **2**, 033397 (2020).
- [37] C. Yue, Y. Xu, Z. Song, H. Weng, Y.-M. Lu, C. Fang, and X. Dai, *Nat. Phys.* **15**, 577 (2019).
- [38] C. Chen, Z. Song, J.-Z. Zhao, Z. Chen, Z.-M. Yu, X.-L. Sheng, and S. A. Yang, *Phys. Rev. Lett.* **125**, 056402 (2020).
- [39] C.-H. Hsu, X. Zhou, T.-R. Chang, Q. Ma, N. Gedik, A. Bansil, S.-Y. Xu, H. Lin, and L. Fu, *Proc. Natl. Acad. Sci. USA* **116**, 13255 (2019).
- [40] C.-H. Hsu, X. Zhou, Q. Ma, N. Gedik, A. Bansil, V. M. Pereira, H. Lin, L. Fu, S.-Y. Xu, and T.-R. Chang, *2D Mater.* **6**, 031004 (2019).
- [41] X. Zhou, C.-H. Hsu, C.-Y. Huang, M. Iraola, J. L. Mañes, M. G. Vergniory, H. Lin, and N. Kioussis, *arXiv:2005.06071*.
- [42] B.-Y. Xie, H.-F. Wang, H.-X. Wang, X.-Y. Zhu, J.-H. Jiang, M.-H. Lu, and Y.-F. Chen, *Phys. Rev. B* **98**, 205147 (2018).
- [43] Z.-G. Chen, C. Xu, R. Al Jahdali, J. Mei, and Y. Wu, *Phys. Rev. B* **100**, 075120 (2019).
- [44] G. Pelegrí, A. M. Marques, V. Ahufinger, J. Mompart, and R. G. Dias, *Phys. Rev. B* **100**, 205109 (2019).
- [45] H. Xue, Y. Yang, F. Gao, Y. Chong, and B. Zhang, *Nat. Mater.* **18**, 108 (2019).

- [46] X. Ni, M. Weiner, A. Alù, and A. B. Khanikaev, *Nat. Mater.* **18**, 113 (2019).
- [47] Z. Liu, *Nat. Mater.* **18**, 98 (2019).
- [48] X. Zhang, B.-Y. Xie, H.-F. Wang, X. Xu, Y. Tian, J.-H. Jiang, M.-H. Lu, and Y.-F. Chen, *Nat. Commun.* **10**, 5331 (2019).
- [49] Z. Zhang, H. Long, C. Liu, C. Shao, Y. Cheng, X. Liu, and J. Christensen, *Adv. Mater.* **31**, 1904682 (2019).
- [50] M. Kim, Z. Jacob, and J. Rho, *Light: Sci. Appl.* **9**, 130 (2020).
- [51] L. Tong, H. Fan, and B. Xia, *J. Phys. D* **53**, 115303 (2020).
- [52] H. Fan, B. Xia, S. Zheng, and L. Tong, *J. Phys. D* **53**, 395304 (2020).
- [53] X.-D. Chen, W.-M. Deng, F.-L. Shi, F.-L. Zhao, M. Chen, and J.-W. Dong, *Phys. Rev. Lett.* **122**, 233902 (2019).
- [54] B.-Y. Xie, G.-X. Su, H.-F. Wang, H. Su, X.-P. Shen, P. Zhan, M.-H. Lu, Z.-L. Wang, and Y.-F. Chen, *Phys. Rev. Lett.* **122**, 233903 (2019).
- [55] H. Xue, Y. Yang, G. Liu, F. Gao, Y. Chong, and B. Zhang, *Phys. Rev. Lett.* **122**, 244301 (2019).
- [56] H. Xue, Y. Ge, H.-X. Sun, Q. Wang, D. Jia, Y.-J. Guan, S.-Q. Yuan, Y. Chong, and B. Zhang, *Nat. Commun.* **11**, 2442 (2020).
- [57] X. Ni, M. Li, M. Weiner, A. Alù, and A. B. Khanikaev, *Nat. Commun.* **11**, 2108 (2020).
- [58] M. Li, D. Zhirihin, M. Gorklach, X. Ni, D. Filonov, A. Slobozhanyuk, A. Alù, and A. B. Khanikaev, *Nat. Photonics* **14**, 89 (2020).
- [59] Z.-K. Lin, H.-X. Wang, Z. Xiong, M.-H. Lu, and J.-H. Jiang, *Phys. Rev. B* **102**, 035105 (2020).
- [60] M. Weiner, X. Ni, M. Li, A. Alù, and A. Khanikaev, *Sci. Adv.* **6**, eaay4166 (2020).
- [61] R. Chen, C.-Z. Chen, J.-H. Gao, B. Zhou, and D.-H. Xu, *Phys. Rev. Lett.* **124**, 036803 (2020).
- [62] A. Agarwala, V. Juričić, and B. Roy, *Phys. Rev. Research* **2**, 012067(R) (2020).
- [63] J.-H. Wang, Y.-B. Yang, N. Dai, and Y. Xu, *Phys. Rev. Lett.* **126**, 206404 (2021).
- [64] Z. Yan, *Phys. Rev. B* **100**, 205406 (2019).
- [65] M. J. Park, Y. Kim, G. Y. Cho, and S. B. Lee, *Phys. Rev. Lett.* **123**, 216803 (2019).
- [66] M. Ezawa, *Phys. Rev. B* **97**, 155305 (2018).
- [67] A. Sil and A. K. Ghosh, *J. Phys.: Condens. Matter* **32**, 205601 (2020).
- [68] Y.-R. Ding, D.-H. Xu, C.-Z. Chen, and X. C. Xie, *Phys. Rev. B* **101**, 041404(R) (2020).
- [69] J. Bao, D. Zou, W. Zhang, W. He, H. Sun, and X. Zhang, *Phys. Rev. B* **100**, 201406(R) (2019).
- [70] H. Yang, Z.-X. Li, Y. Liu, Y. Cao, and P. Yan, *Phys. Rev. Research* **2**, 022028(R) (2020).
- [71] Y.-L. Tao, N. Dai, Y.-B. Yang, Q.-B. Zeng, and Y. Xu, *New J. Phys.* **22**, 103058 (2020).
- [72] Y. You, T. Devakul, F. J. Burnell, and T. Neupert, *Phys. Rev. B* **98**, 235102 (2018).
- [73] V. Dwivedi, C. Hickey, T. Eschmann, and S. Trebst, *Phys. Rev. B* **98**, 054432 (2018).
- [74] H. Chen and X. C. Xie, *Phys. Rev. A* **100**, 013601 (2019).
- [75] K. Kudo, T. Yoshida, and Y. Hatsugai, *Phys. Rev. Lett.* **123**, 196402 (2019).
- [76] X.-W. Xu, Y.-Z. Li, Z.-F. Liu, and A.-X. Chen, *Phys. Rev. A* **101**, 063839 (2020).
- [77] A. L. Szabó, R. Moessner, and B. Roy, *Phys. Rev. B* **101**, 121301(R) (2020).
- [78] A. Rasmussen and Y.-M. Lu, *Phys. Rev. B* **101**, 085137 (2020).
- [79] E. Edvardsson, F. K. Kunst, and E. J. Bergholtz, *Phys. Rev. B* **99**, 081302(R) (2019).
- [80] M. Ezawa, *Phys. Rev. B* **99**, 121411(R) (2019).
- [81] M. Ezawa, *Phys. Rev. B* **99**, 201411(R) (2019).
- [82] B. Roy, *Phys. Rev. Research* **1**, 032048(R) (2019).
- [83] X.-W. Luo and C. Zhang, *Phys. Rev. Lett.* **123**, 073601 (2019).
- [84] T. Liu, Y.-R. Zhang, Q. Ai, Z. Gong, K. Kawabata, M. Ueda, and F. Nori, *Phys. Rev. Lett.* **122**, 076801 (2019).
- [85] Z. Zhang, M. Rosendo López, Y. Cheng, X. Liu, and J. Christensen, *Phys. Rev. Lett.* **122**, 195501 (2019).
- [86] J. Pan and L. Zhou, *Phys. Rev. B* **102**, 094305 (2020).
- [87] H. Araki, T. Mizoguchi, and Y. Hatsugai, *Phys. Rev. B* **99**, 085406 (2019).
- [88] R. Seshadri, A. Dutta, and D. Sen, *Phys. Rev. B* **100**, 115403 (2019).
- [89] Y. Otaki and T. Fukui, *Phys. Rev. B* **100**, 245108 (2019).
- [90] Z. Li, Y. Cao, P. Yan, and X. Wang, *npj Comput. Mater.* **5**, 107 (2019).
- [91] A. El Hassan, F. K. Kunst, A. Moritz, G. Andler, E. J. Bergholtz, and M. Bourennane, *Nat. Photonics* **13**, 697 (2019).
- [92] Q. Wang, C.-C. Liu, Y.-M. Lu, and F. Zhang, *Phys. Rev. Lett.* **121**, 186801 (2018).
- [93] T. Nag, V. Juričić, and B. Roy, *Phys. Rev. Research* **1**, 032045(R) (2019).
- [94] A. K. Ghosh, G. C. Paul, and A. Saha, *Phys. Rev. B* **101**, 235403 (2020).
- [95] B. Huang and W. V. Liu, *Phys. Rev. Lett.* **124**, 216601 (2020).
- [96] H. Hu, B. Huang, E. Zhao, and W. V. Liu, *Phys. Rev. Lett.* **124**, 057001 (2020).
- [97] A. K. Ghosh, T. Nag, and A. Saha, *Phys. Rev. B* **103**, 085413 (2021).
- [98] A. K. Ghosh, T. Nag, and A. Saha, *Phys. Rev. B* **103**, 045424 (2021).
- [99] T. Nag, V. Juričić, and B. Roy, *Phys. Rev. B* **103**, 115308 (2021).
- [100] A. K. Ghosh, T. Nag, and A. Saha, [arXiv:2104.12441](https://arxiv.org/abs/2104.12441).
- [101] F. D. M. Haldane, *Phys. Rev. Lett.* **61**, 2015 (1988).
- [102] N. Marzari and D. Vanderbilt, *Phys. Rev. B* **56**, 12847 (1997).
- [103] A. A. Soluyanov and D. Vanderbilt, *Phys. Rev. B* **83**, 035108 (2011).
- [104] H. C. Po, A. Vishwanath, and H. Watanabe, *Nat. Commun.* **8**, 50 (2017).
- [105] B. Bradlyn, L. Elcoro, J. Cano, M. G. Vergniory, Z. Wang, C. Felser, M. I. Aroyo, and B. A. Bernevig, *Nature (London)* **547**, 298 (2017).
- [106] Z. Song, Z. Fang, and C. Fang, *Phys. Rev. Lett.* **119**, 246402 (2017).
- [107] R. Resta, *Ferroelectrics* **136**, 51 (1992).
- [108] R. D. King-Smith and D. Vanderbilt, *Phys. Rev. B* **47**, 1651 (1993).
- [109] R. Resta, *Rev. Mod. Phys.* **66**, 899 (1994).

- [110] V. M. Pereira, A. H. Castro Neto, and N. M. R. Peres, *Phys. Rev. B* **80**, 045401 (2009).
- [111] See Supplemental Material at <http://link.aps.org/supplemental/10.1103/PhysRevB.104.L121108> for details.
- [112] S. Ryu and Y. Hatsugai, *Phys. Rev. Lett.* **89**, 077002 (2002).
- [113] G. Jotzu, M. Messer, R. Desbuquois, M. Lebrat, T. Uehlinger, D. Greif, and T. Esslinger, *Nature (London)* **515**, 237 (2014).
- [114] W. Liu, Z. Lin, Z. D. Wang, and Y. Chen, *Sci. Rep.* **8**, 12898 (2018).
- [115] R.-B. Liu, D.-L. Deng, D.-W. Zhang, and S.-L. Zhu, *J. Opt. Soc. Am. B* **32**, 2500 (2015).
- [116] S. Lannebère and M. G. Silveirinha, *Nanophotonics* **8**, 1387 (2019).
- [117] W.-Y. He, S. Zhang, and K. T. Law, *Phys. Rev. A* **94**, 013606 (2016).